Site-Resolved Neutralization of Slow Singly and Multiply Charged Ions during Large-Angle Backscattering Collisions with RbI(100)

F. W. Meyer, H. F. Krause and C. R. Vane

Physics Division, Oak Ridge National Laboratory

Oak Ridge, Tennessee 37831-6372 USA

Abstract

Preliminary results are reported of projectile neutralization during 120^0 backscattering from RbI[100] of singly and multiply charged incident ions in the keV energy range. Scattered charge fractions are reported for 4.4 keV Ne^{8+} and 4.2 keV F^+ normally incident on the ionic crystal. Collisions associated with scattering from a Rb or I site can be clearly distinguished for each scattered final charge state. Significant differences are observed in the intensities of the higher scattered charge states resulting from collisions with Rb and I sites. In contrast, at the target azimuth orientation of the present measurement, only minor differences in F^- yield are observed for hard scattering from the two lattice sites.

PACS numbers: 79.20.Rf, 79.20.Ap, 34.50 Dy, 61.18.Bn

*Corresponding author: FAX: +1-1-865-574-1118

E-mail address: meyerfw@ornl.gov

1. Introduction

The large-angle backscattering technique has seen increased use in studies of multicharged ion (MCI) neutralization during interactions with solid surfaces[1-7]. The use of MCI projectiles has been shown to significantly enhance the surface sensitivity of the backscattering technique [3]. Also, in contrast to grazing incidence studies where a large number of lattice sites are involved [8], large-angle backscattering measurements allow the resolution of interactions occurring with just one or two atoms located on the target surface.

Simultaneous energy and charge-state analysis of the backscattered projectiles have provided insights into energy loss mechanisms accompanying projectile neutralization leading to particular final charge states [1,2]. More recently, the large-angle backscattering technique has provided information on site-specific MCI neutralization at a Au(110) surface. In the latter work, a strong target azimuth dependence was observed in the scattered projectile charge state distributions. Extensive trajectory simulations performed in conjunction with the measurements were able to reproduce the observed variations with target azimuth, and provided a framework for demonstrating differences in MCI neutralization at the different scattering sites on the corrugated Au(110) metal surface [3,7].

We have recently extended such studies to insulator targets by measuring projectile backscattering from RbI(100). Goals of this work are to identify and understand differences in final charge-state distributions and neutralization mechanisms that occur on ordered insulator and metal surfaces. RbI(100) was chosen in the hope of obtaining site-resolved projectile neutralization information at Rb and I lattice sites. Due

to their significant mass difference, large-angle backscattering from the two lattice sites should lead to sufficiently different elastic binary collision energy losses to be resolvable using our time-of-flight (TOF) energy analysis technique.

2. Experiment

The measurements were performed at the ORNL Multicharged Ion Research Facility (MIRF) using an ultra high vacuum (10^{-10} mbar) apparatus previously described [2]. A chopped primary ion beam is decelerated from (10 x q) keV to final energies in the range 4 - 5 keV before impinging on a single crystal RbI(100) surface. The crystal is attached to a goniometer that has two rotational degrees of freedom. A TOF analyzer, located 120^0 from the incident beam direction, registers projectiles scattered from the crystal surface using a multichannel plate (MCP) detector. The TOF analyzer, which has a floatable drift tube, allows simultaneous measurement of energy distributions and charge fractions for the scattered ions [2]. Time zero calibration was obtained from the soft x-ray peak registered on the TOF detector resulting from projectile impact on the surface in the case of highly charged ions, or from the secondary electron peak observed when the flight tube and MCP detector were biased a few hundred volts positive. The RbI(100) surface was prepared by cycles of sputter cleaning under grazing incidence conditions using 2 keV Ar^+ ions and successive annealing at about 450^0 C. To prevent macroscopic charging, the RbI target was maintained at a temperature of 250^0 C during the measurements.

The energy-loss technique enables identification of the binary collision partner causing the large-angle backscattering at the surface. When a projectile of energy E_0

(mass = m_p) elastically scatters from a target atom at rest (mass = m_t), the projectile recoil energy E_r depends on the scattering angle _ as

$$E_r = E_0 \{ [\_\cos \_ + (1- \_^2 \sin^2 \_)^{1/2}] / (1 + \_) \}^2 \quad , \qquad (1)$$

where $\mu = m_p / m_t < 1$. A 120^0 scattering event ("hard" collision), which is associated with a small impact parameter collision (e.g., $\rho_b \sim 0.004$ nm), results in a substantial energy loss. When the surface has two constituents of significantly different masses (e.g., Rb and I), hard collisions at the two sites give rise to different recoil energies that can be resolved experimentally in our TOF apparatus (site specificity for each final charge state). In contrast, for a possible subsequent small-angle scattering event (i.e., "soft" collision, $\rho >> \rho_b$) on the receding trajectory, very little energy is lost in a collision with either Rb or I. Therefore, a "quasi-binary " double scattering event ("hard-soft" collision sequence) can have an energy loss close to that of a single "hard" collision. Interesting possibilities arise when an ionic crystal such as RbI is examined with this technique.

RbI has a diatomic cubic structure (rock salt) of alternating atoms ABAB on each side of the unit cell (e.g., the <100> direction, with 0.366 nm atomic spacing). In the <110> direction, there are alternating parallel atomic rows AAAA and BBBB (0.517 nm atomic spacing). Thus, azimuthal rotation of the crystal (resulting in alignment of the scattering plane, e.g., with the <100> or the <110> directions) changes the adjacent atomic species and their atomic spacing. Moreover, interaction with widely spaced A_B_A_B atomic strings (0.818 nm spacing) can be selected when the scattering plane is aligned with the <210> direction. These features are illustrated in Figure 1, which shows the present scattering geometry for normal incidence conditions along two

different target azimuths, when the hard scattering site is iodine (the corresponding case where rubidium is the hard collision site is not shown). It is evident from Fig. 1 that for the RbI(100) surface, hard collisions with deeper layers are “blocked” under normal incidence conditions. The goal of the present experiment is to employ the relative intensities for binary scattering associated with Rb and I sites as a "signature" for identifying and probing neutralization pathways in these different orientation-dependent "quasi-binary" collision sequences. In the preliminary results presented below, scattered charge fractions observed for incident Ne^{8+} and F^{+} ions measured for normal incidence and a single target orientation will be shown. A more complete presentation of all measurements obtained at other target azimuth orientations and incidence conditions will be deferred pending completion of data analysis similar to that presented in Section 4 below.

3. Results

We present illustrative results of scattered projectile charge fractions for 120^0 backscattering of 4.2 keV F^{+} and 4.4 keV Ne^{8+} normally incident on RbI(100) at a single target azimuth. Fig. 2 shows a raw TOF spectrum for normally incident 4.2 keV F^{+} ions in a plane about 30^0 from the <100> direction of the RbI(100) surface, obtained with the floating TOF drift tube biased at – 3 kV. Backscattered F^{+} ions are separated in flight time from scattered F^0 due to post-acceleration in the biased TOF drift tube. Binary collision peaks associated with backscattering from Rb and I sites are clearly resolved for both the neutral and 1+ final charge states. The scattered neutral binary collision peaks sit on top of a broad background structure; it arises from multiple collisions whose trajectories extend deeper into the RbI bulk prior to exiting toward the TOF analyzer.

The TOF spectrum shown in Fig. 3 was obtained for the same incident ion and scattering geometry as Fig. 2, but with the flight tube biased at + 3 kV. Because this bias voltage is greater than the energy of the backscattered F^+ ions, only scattered F^0 and F^- are detected. The two components are separated in flight time by the post-acceleration of the F^- ions in the now positively biased TOF drift tube. Clearly resolved binary collision peaks, associated with hard collisions with Rb and I scattering sites, are observed for F^0 and F^- scattered charge states (see Fig. 3). The F^- binary collision peaks sit on top of a broad background structure, which extends to, and overlaps with the neutral multiple collision background noted in Fig. 2. The F^- multiple collision background is closely related to the F^0 background, and results from F^- formation from multiply scattered F^0 particles as they exit the surface toward the TOF analyzer, a process that occurs with high probability. In contrast, re-ionization of multiply scattered F^0 particles as they exit the RbI surface is much less likely at 4.2 keV. This results in the barely discernable F^+ multiple collision background in the vicinity of the scattered F^+ binary collision peaks of Fig. 2.

A representative TOF spectrum for a highly charged incident ion is shown in Fig. 4. The data shown is for 4.4 keV Ne^{8+} ions normally incident on RbI(100) along the <100> direction of the lattice, and was acquired with a TOF drift tube bias voltage of –3 kV. Clearly resolved binary collision peak Rb/I doublets are seen for charge states as high as 3+. In contrast to the F^+ incident ions shown in Figs. 2 and 3, the neutral scattered component appears to be comprised largely of a broad multiple collision background. An estimate of the binary collision scattered neutrals that can be extracted from this spectrum will be provided in the next section. The small peak observed at t=0, due to soft x-ray

photons produced by projectile impact on the surface, was used to calibrate the flight time scale. A bias voltage of +400V was applied to a grid immediately in front of the biased TOF drift tube, in order to suppress slow secondary ions whose presence would otherwise create significant backgrounds over the entire flight time range shown in Fig. 4.

4. Data Analysis

To obtain quantitative results of scattered charge fractions from the spectra shown in Figs. 2-4, the raw TOF spectra are converted to energy spectra. This conversion takes into the account the geometry of the TOF analyzer, and the voltages applied to the drift tube and various grids (including that used to reject slow secondary ions), which cause charge state-dependent variations in detector collection efficiency, as has been discussed previously [2]. The corrections can be significant and must be properly accounted for in an accurate determination of scattered charge fractions.

Figs. 5 and 6 show the energy spectra derived from the TOF spectra of Figs. 2 and 3. The observed Rb/I binary collision peak energies correspond closely to the energies of 2.13 and 2.67 keV, respectively, calculated from Equ. 1 for 120^0 backscattering from Rb and I. The F^- binary collision peaks shown in Fig. 6 have been background subtracted, and thus do not show the multiple collision background evident in Fig. 3. Using a non-linear fitting routine based on Gaussian peak shapes, peak areas were determined for the F^+, F^0, and F^- scattered charge components. These areas were used in turn to determine the scattered charge fractions for hard collisions with Rb and I lattice sites. The results are summarized in Table I. When summed over all final scattered charge states, the ratio of total scattered binary collision intensities from Rb and I sites was determined to be 0.6.

The energy-transformed spectra of the different scattered charge states for the Ne^{8+} incident projectiles are shown in Fig. 7. Again, the observed peak energies for Rb and I scattering are in good agreement with those calculated according to Equ. 1 (2.15 and 2.73 keV, respectively). Individual peak areas were determined using a multi-Gaussian fitting routine. As noted previously, the neutral binary collision peaks for incident Ne^{8+} are not prominent above the multiple collision background. However, after some smoothing and with knowledge of the peak energies as determined from the charged scattered components, a deconvolution of the neutral shape, and extraction of binary collision peaks was possible using a non-linear peak fitting algorithm, albeit with less precision than was possible with the charged components. This deconvolution is shown in Fig. 8, and is estimated to provide an upper bound to the scattered binary collision neutral component. Using the thus determined peak areas of all the charge states, the scattered charge fractions for incident Ne^{8+} were calculated. They are summarized in Table II below. The total scattered binary collision intensity ratio for Rb and I sites was determined to be 0.65.

5. Discussion

Regarding the incident 4.2 keV F^+ projectile scattered charge fraction result, the large negative F ion yield is particularly noteworthy. Large negative ion yields have been previously reported for grazing interactions with alkali halide targets [9]. For such insulator targets, the Coulomb attraction between the receding F^- and the positively charged hole left in the surface is thought to be the dominant mechanism that brings about a sufficient “confluence” of initial and final state energy levels that negative ion production becomes possible. Nevertheless, calculations [10] indicate that, at least for a

LiF target, a large number of glancing interactions with halogen sites may be required to accumulate sufficient negative ion population buildup to agree with experiment. In the present case, after a single hard collision causing the 120^0 backscattering, the projectile recedes from the surface at an angle of 30^0. The next neighbor interaction on the receding trajectory has an impact parameter of about 3.5 a_0, which doubles with each succeeding encountered site, so that grazing charge transfer with more than 2 subsequent sites does not appear likely. Alternatively, F^- could be produced in the 120^0 backscattering collision directly from incident F^+, but this possibility would require an explanation of the large F^- yield even for a hard collision with a Rb^+ site, which, unlike the I^- sites, has no loosely bound electrons to transfer.

We have made measurements of negative F formation from incident F^+ at non-normal incidence angles, which result in more grazing receding trajectories (down to about 10^0 with respect to the surface plane). Inspection of the raw data suggests even larger negative ion yields for these cases, and shows significant variations with target azimuth orientation, but detailed analyses of these measurements is not yet completed. Nevertheless, the approach of studying “half-grazing” collisions in this manner may provide a useful probe of the distances at which negative ion formation is still possible. The importance of additional active mechanisms such as trion formation [11] and correlated double capture from adjacent halogen sites [12] may play a role as well and will need to be assessed for the present scattering geometry.

Regarding the scattered charge fraction results for incident Ne^{8+}, at least two things can be noted. The first is the strongly reduced binary collision neutral peaks in comparison with the F^+ incident ion spectrum of Fig. 2, which features prominent binary

collision neutral components. This reduction in neutral binary collision intensity is a shared feature of all the spectra measured for MCI incident on RbI(100), as well as of our earlier measurements on CsI(100)[6]. This feature is in strong contrast to our measurements on Au(110), where binary collision neutrals were the dominant scattered charge state for all incident charge states investigated [3,7]. One possible reason for the decreased neutralization observed for the alkali halide targets is that the collision time may be significantly shorter than the lattice-site reneutralization time ("hole hopping" time [13]). The reduced target Z of the two scattering sites and the absence, in large part, of delocalized electrons in RbI in comparison to Au are additional factors to be considered in arriving at an explanation of the reduced binary collision neutral yield observed for the RbI target.

A second notable feature is the significantly smaller yields of the higher scattered charge states obtained for the case of backscattering from Rb in comparison to the backscattering from I. As seen in Table II, the difference amounts to almost a factor of three for scattered 3+ ions. This is a counter-intuitive result, since the difference in Z between the two scattering centers (37 vs. 53) and the fact that the loosely bound target valence electrons are localized about the I sites would seem to support arguments for the opposite trend.

As was already noted in connection with the F^+ incident results, a detailed incidence angle and target azimuth dependence study was carried out for the multiply charged incident ions as well. Inspection of the raw spectra shows significant dependence of the scattered charge state distributions on both variables. The indications of a target azimuth dependence suggest again that "hard-soft" quasi-binary double collisions may be

a significant determinant of MCI projectile neutralization during backscattering from insulators, similar to our earlier results for Au(110). To assess the importance of such collisions, detailed MARLOWE trajectory simulations [14] are planned using the formalism and approach developed previously for the analysis of our Au (110) results.

A final remark is in order regarding the noted total Rb/I scattered intensity ratios determined from the analysis of our incident F^+ and Ne^{8+} discussed in Section 4. For both incident ions, the experimental intensity ratios lie within the estimated experimental uncertainty of about 20% of the theoretical ratio of the differential scattering cross sections [15] at 120^0 for Rb and I for a screened Coulomb potential. This finding is consistent with our earlier observation [3] for Au(110), that the target azimuthal variations of measured scattered flux intensities for incident MCI were well reproduced by Monte Carlo classical trajectory simulations which used a charge-state independent ZBL screened Coulomb potential. The agreement with the theoretical differential scattering cross section ratios at the 20% level further reinforces our earlier noted evidence that hard-collision backscattering and projectile neutralization occur in mutually independent ways (or, at least, can be considered separately). The basis for this intriguing finding will be explored in greater detail in upcoming experiments.

6. Acknowledgements

This research was sponsored in part by the Office of Fusion Energy Sciences and by the Office of Basic Energy Sciences of the U. S. Department of Energy under contract No. DE-AC05-00OR22725 with UT-Battelle, LLC.

References

[1] W. Huang, H. Lebius, R. Schuch, M. Grether, and N. Stolterfoht, Phys. Rev. **A58**, 2962 (1998).

[2] V.A. Morozov and F.W. Meyer, Rev. Sci. Inst. **70**, 4515 (1999).

[3] V.A. Morozov and F.W. Meyer, Phys. Rev. Lett. **86**, 736 (2001).

[4] V.A. Morozov and F.W. Meyer, Phys. Scripta **T92**, 31 (2001).

[5] F. W. Meyer, V.A. Morozov, R.C. Vane, and S. Datz, Phys. Scripta **T92**, 182 (2001).

[6] F. W. Meyer, V. A. Morozov, J. Mrogenda, C. R. Vane, and S. Datz, Nucl. Instr. Methods Phys. Res. **B193,** 508 (2002).

[7] F. W. Meyer and V. A. Morozov, Nucl. Instr. Methods Phys. Res. **B193,** 530 (2002).

[8] F.W. Meyer, Q. Yan, P. Zeijlmans van Emmichoven, I.G. Hughes, and G. Spierings, Nucl. Instr. Methods Phys. Res. **B125,** 138 (1997).

[9] C. Auth, A. Mertens, H. Winter, A. G. Borisov, and V. Sidis, Phys. Rev. **A57**, 351(1996).

[10] A. G. Borisov, and V. Sidis, Phys. Rev. **B56**, 10628 (1997).

[11] H. Khemliche, J. Villette, A. G. Borisov, A. Momeni, and P. Roncin, Phys. Rev. Lett. **86**, 5699(2001).

[12] P. Roncin, A. G. Borisov, H. Khemliche, A. Momeni, A. Mertens, and H. Winter, Phys. Rev. Lett. **89**, 043201-1(2002).

[13] L. Wirtz, C. Lemell, C. O. Reinhold, L. Hägg, and J. Burg_rfer, Nucl. Instr. Methods Phys. Res. **B182,** 36 (2001).

[14] M.T. Robinson, Radiat. Eff. Defect. Solid. **130**, 3 (1994).

[15] M.T. Robinson, Tables of Classical Scattering Integrals, ORNL-4556, (1970)

Figure captions

Fig. 1. Schematic diagram of scattering geometry using a Rb(100) single crystal.

Fig. 2. Raw TOF spectrum of 120^0 backscattering of 4.2 keV F^+ ions from RbI(100) in a plane roughly 30^0 away from the <100> direction, showing neutral and positive scattered charge states; TOF drift tube voltage was – 3 kV.

Fig. 3. Raw TOF spectrum of 120^0 backscattering of 4.2 keV F^+ ions from RbI(100) in a plane roughly 30^0 away from the <100> direction, showing neutral and negative scattered charge states; TOF drift tube voltage was + 3 kV.

Fig. 4 . Raw TOF spectrum for normal incidence 4.4 keV Ne^{8+} ions scattered along the <100> direction of RbI (100); TOF drift tube voltage was – 3 kV.

Fig. 5. Energy spectra of scattered F^+ and F^0 produced from incident 4.2 keV F^+ projectiles, obtained from Figure 2.

Fig. 6. Energy spectra of scattered F^- and F^0 produced from incident 4.2 keV F^+ projectiles, obtained from Figure 3.

Fig. 7. Energy spectra of scattered neutral and positively charged ions for incident 4.4 keV Ne^{8+} projectiles, obtained from Figure 4.

Fig. 8. Deconvolution of the scattered neutral component for incident Ne^{8+} projectiles, showing fitting results for the binary collision peaks originating from Rb and I sites.

Table I: Scattered charge fractions 120^0 backscattered from Rb and I, respectively, for 4.2 keV F^+ normally incident on RbI(100).

Scattered charge state	Rb(%)	I(%)
1+	15	12
neutrals	45	45
-1	40	43

Table II: Scattered charge fractions 120^0 backscattered from Rb and I, respectively, for 4.4 keV Ne^{8+} normally incident on RbI(100).

Scattered charge state	Rb scattering (%)	I scattering (%)
Neutrals	40	34
1+	44	46
2+	15	18
3+	0.8	2.1

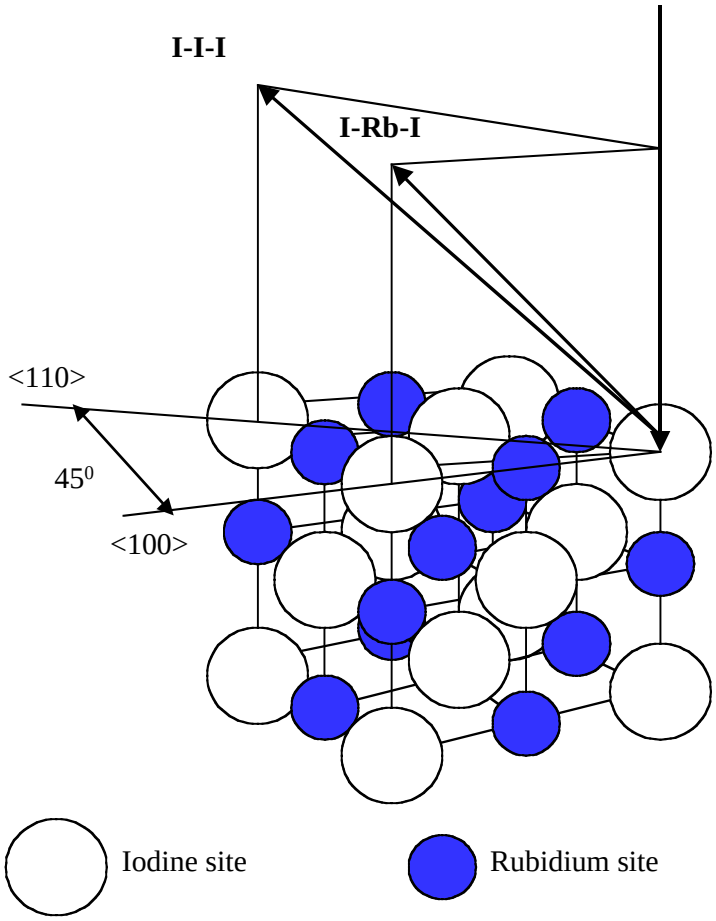

Figure 1

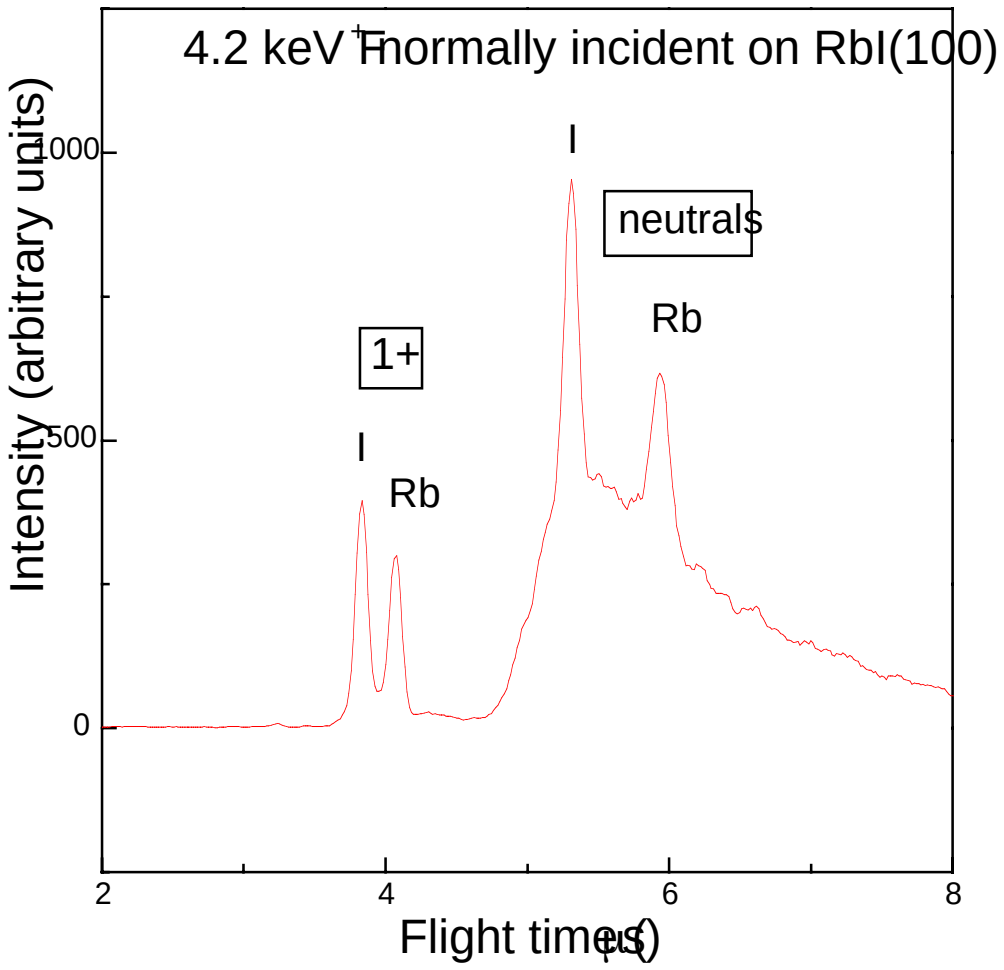
4.2 keV I+ normally incident on RbI(100)
Intensity (arbitrary units)
1000
500
0
I
Rb
1+
I
neutrals
Rb
2
4
6
8
Flight times (μs)

Figure 2

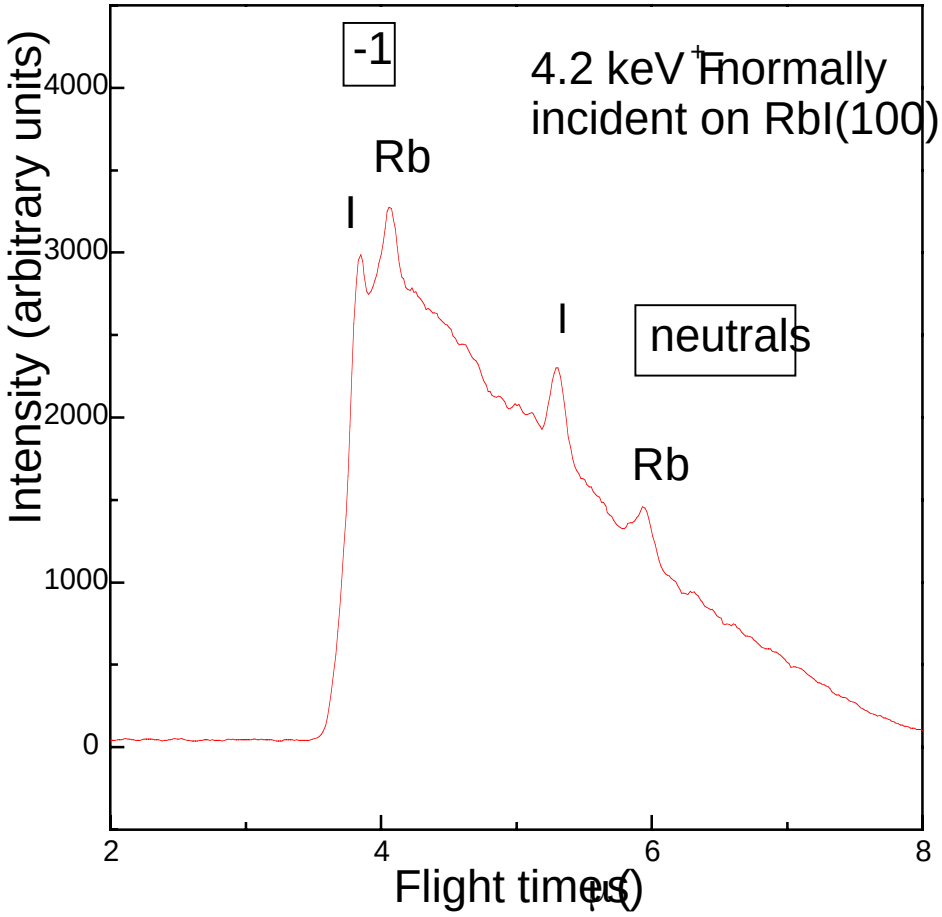
-1
4.2 keV F+ normally
incident on RbI(100)
Rb
I
I
neutrals
Rb
Intensity (arbitrary units)
4000
3000
2000
1000
0
2
4
6
8
Flight times (μs)

Figure 3

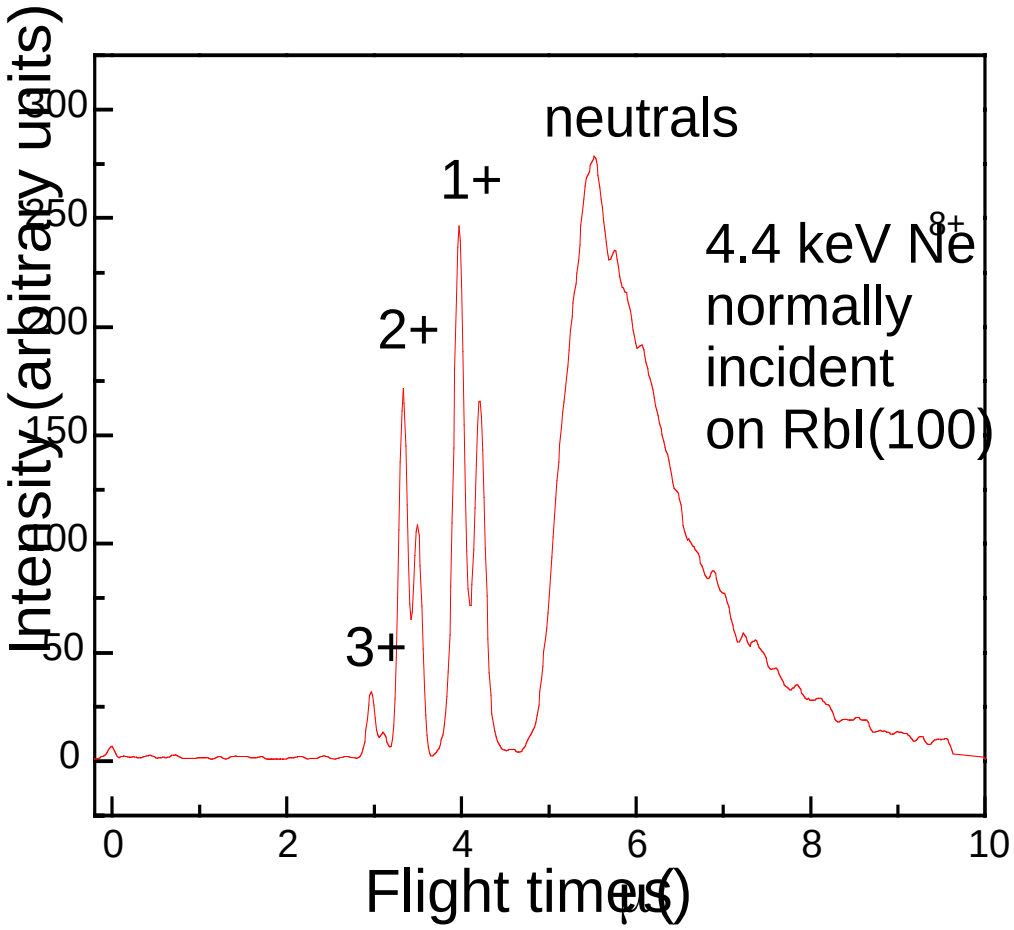
neutrals
1+
2+
3+
4.4 keV Ne8+
normally
incident
on RbI(100)
Intensity (arbitrary units)
Flight times (μs)
0
50
100
150
200
250
300
0
2
4
6
8
10

Figure 4

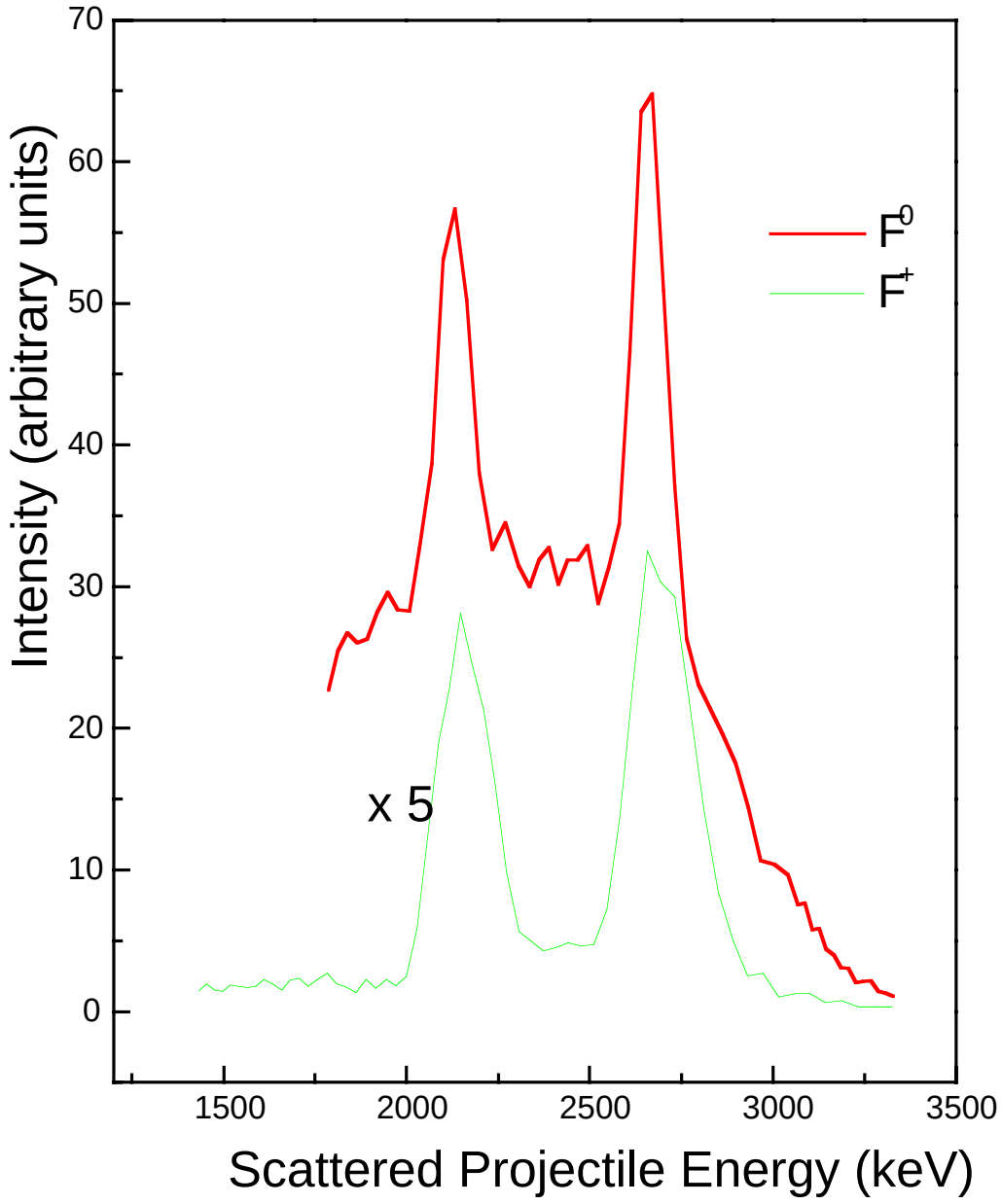
70
60
50
40
30
20
10
0
Intensity (arbitrary units)
1500
2000
2500
3000
3500
Scattered Projectile Energy (keV)
F0
F+
x 5

Figure 5

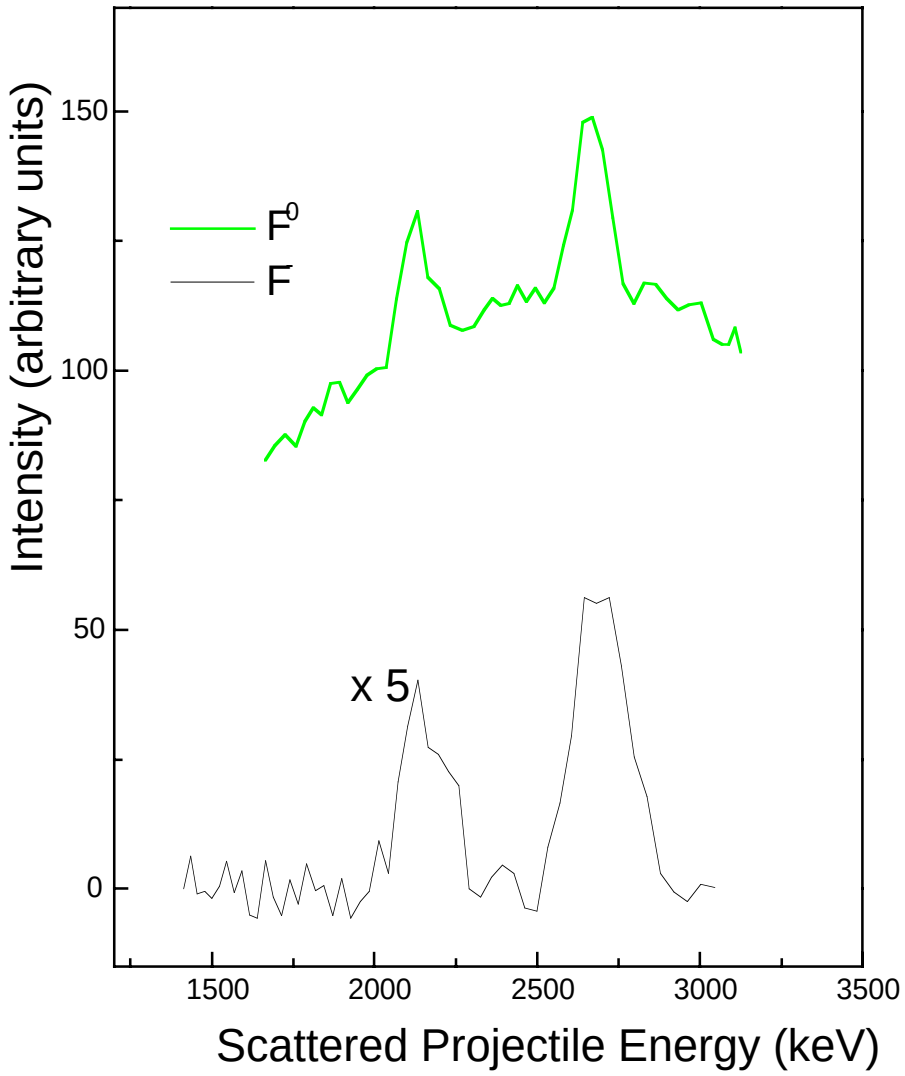
Intensity (arbitrary units)
150
100
50
0
F0
F-
x 5
1500
2000
2500
3000
3500
Scattered Projectile Energy (keV)

Figure 6

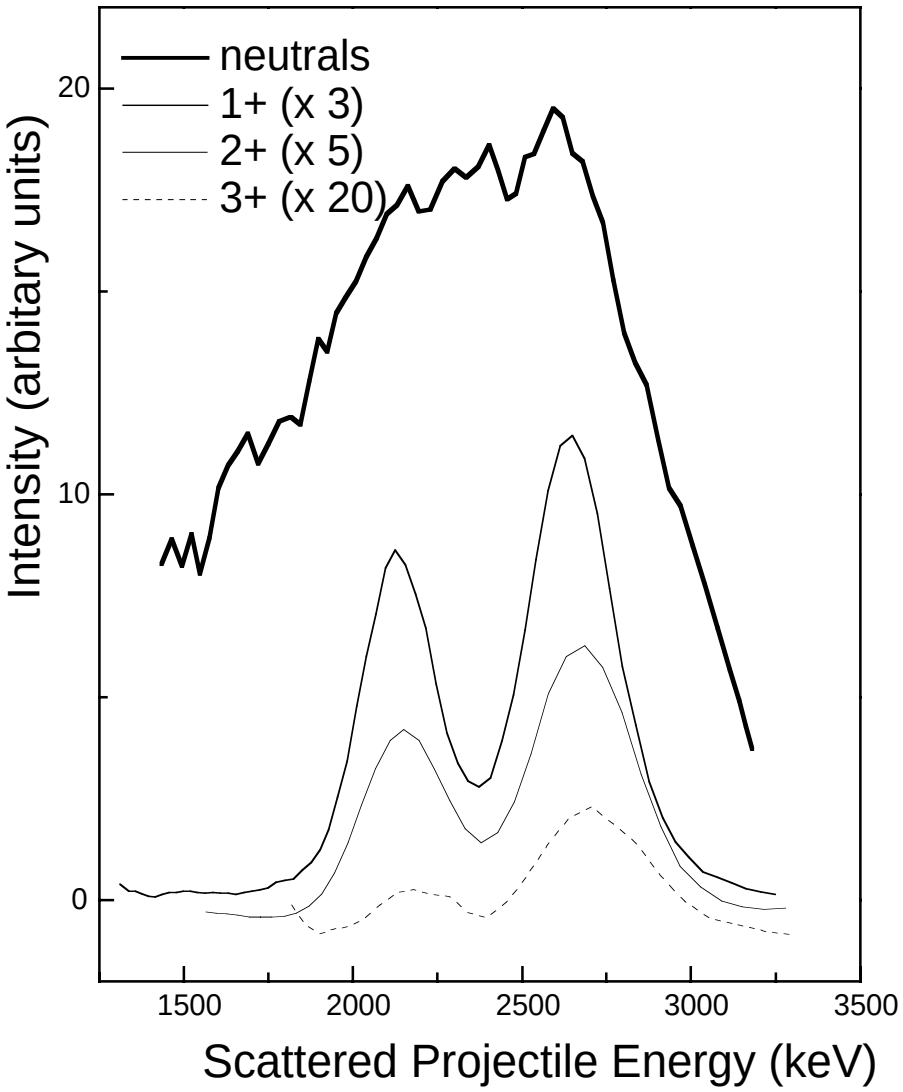
neutrals
1+ (x 3)
2+ (x 5)
3+ (x 20)
Intensity (arbitary units)
0
10
20
1500
2000
2500
3000
3500
Scattered Projectile Energy (keV)

Figure 7

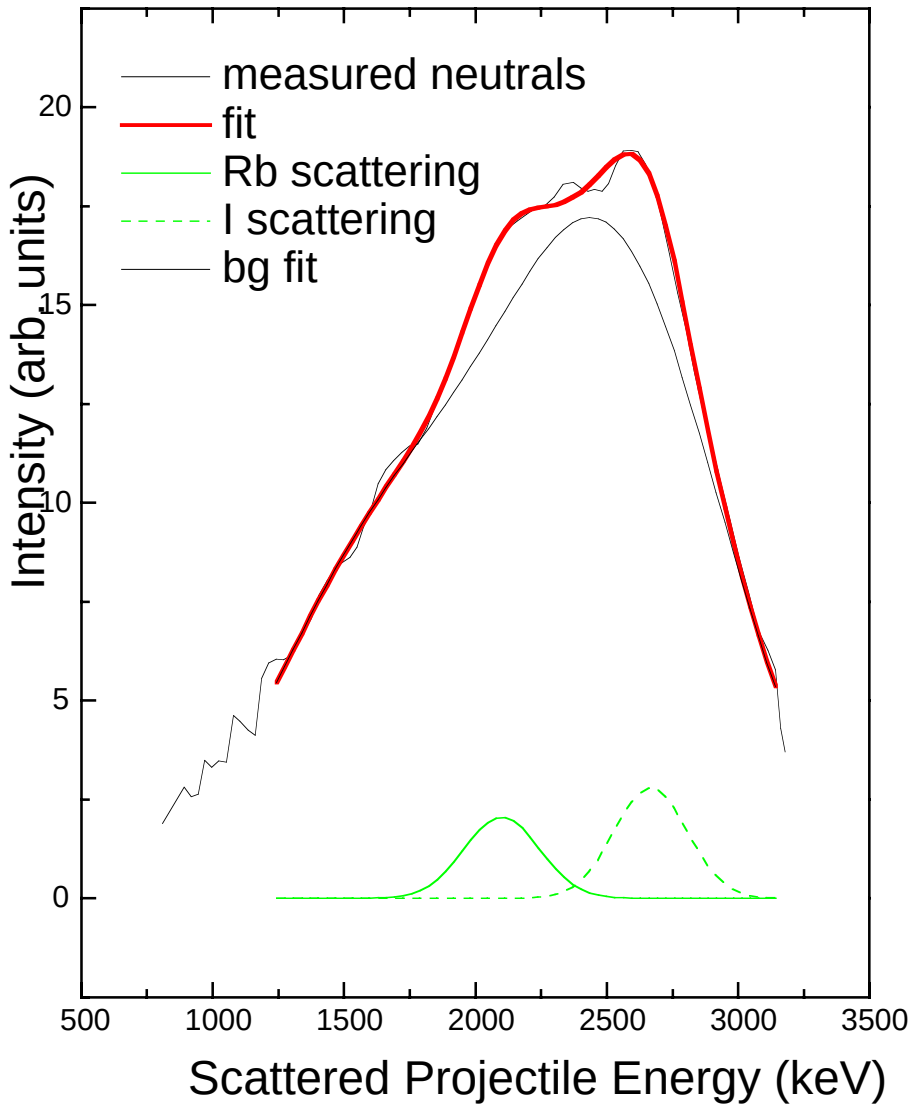
measured neutrals
fit
Rb scattering
I scattering
bg fit
Intensity (arb. units)
0
5
10
15
20
500
1000
1500
2000
2500
3000
3500
Scattered Projectile Energy (keV)

Figure 8